

https://doi.org/10.1070/QEL17197

Simulation of femtosecond interferometry when studying the effect of intense laser irradiation of a transparent medium

E.V. Zavedeev, V.V. Kononenko, V.M. Gololobov, V.I. Konov

Abstract. **A method for comparing experimental and simulation results obtained when transmitting a femtosecond laser pulse through a material is proposed. This method is based on computer reproduction of photographs recorded using femtosecond interferometry. A numerical analysis of the spatial and temporal evolution of an intense ($\sim 10^{13}$ W cm^{-2}) pulse propagating in the bulk of yttrium aluminium garnet is presented.**

Keywords: *femtosecond laser radiation, fast processes in solids, femtosecond interferometry.*

1. Introduction

The possibility of bulk laser structuring of transparent materials stimulates undiminishing interest of researchers in the processes of interaction of high-power radiation with solids. Nonlinear absorption in the focal waist region may cause strong excitation of material and lead to its permanent modification (e.g., densification [1], colouration [2], allotropic transformation [3, 4], amorphisation [5], nanoscale structurisation [6]) or destruction [7]). Note that nonlinear interaction of radiation with a medium changes significantly the propagation path, as well as the spatial and temporal shape of intense ultrashort laser pulse focused in the bulk of material. Actual is the problem of measuring, predicting, and controlling the light-induced excitation of a medium.

Femtosecond interferometry [8, 9] is a convenient tool for such measurements, because it allows one to estimate the change in the refractive index in the laser-irradiated region. The data obtained with this method contain information about the local radiation intensity, density of excited free carriers and transient bound states, etc. In essence, an interference photograph is a spatial and temporal convolution of the distribution of light-induced change in the refractive index (Δn) and the electromagnetic field of probe pulse in the material. The spatial resolution of interferometric images is limited by the diffraction limit, while the temporal resolution is determined by the pulse width.

E.V. Zavedeev, V.V. Kononenko, V.M. Gololobov, V.I. Konov
Prokhorov General Physics Institute, Russian Academy of Sciences, ul. Vavilova 38, 119991 Moscow, Russia; National Research Nuclear University MEPhI, Kashirskoe shosse 31, 115409 Moscow, Russia; e-mail: dodeskoden@gmail.com; vitali.kononenko@gmail.com; gololobov@physics.msu.ru; vik@nsc.gpi.ru

Received 24 November 2019; revision received 12 December 2019
Kvantovaya Elektronika **50** (2) 175–178 (2020)
Translated by Yu.P. Sin'kov

To interpret the information present in interference photographs, one must perform their deconvolution. However, deconvolution is an ill-posed problem, i.e., a problem in which small errors in the initial data lead to a strong distortion of the solution. Since interference photographs contain a rather large number of artefacts (related to optical system aberrations, matrix noises, and probe beam diffraction), one can hardly directly extract information about the field distribution and the state of the medium from them; this is a hindrance for direct comparison of theoretical and experimental data.

Previously, a method based on comparing the dynamics of probe-beam phase shift $\Delta\varphi(t)$ at a chosen point of optical axis [10] was proposed to correlate the results of numerical simulation and femtosecond interferometry data. Theoretical dependences were obtained by integrating the calculated Δn value. A drawback of this method is the use of only a small amount of data (related to a given point) from all the dataset.

In this paper we consider an alternative method for comparing simulation and experimental femtosecond interferometry data. Computer reproduction of interferometric images is performed based on calculations, and then reproduced images are compared with experimental ones. The applicability of this method is evaluated by an example of propagation of a femtosecond laser pulse in yttrium aluminium garnet (YAG).

2. Experimental

The radiation source was a 800-nm Tsunami Ti:sapphire laser (Spectra Physics) equipped with a regenerative Spitfire amplifier (Spectra Physics). The pulse width was 140 fs. A pump pulse was focused by an aspherical lens with a focal length $f = 30$ mm in a polished YAG sample at a depth of 300 μm from the surface.

The induced polarisability of the medium was studied by femtosecond interferometry. A probe beam passed (after a delay line) through the focal waist of the pump beam perpendicular to its optical axis. An objective (NA = 0.40) and a lens ($f = 500$ mm), arranged in a telescope configuration, were used to image the focal region on a CCD matrix. After the telescope the parallel probe beam passed through a Sagnac interferometer, which formed a broadband interference pattern. The inset in Fig. 1 presents two images corresponding to different interferometer arms. A local change in the refractive index in the irradiated region caused a local phase shift of the probe beam wavefront, which, in turn, led to a change in the brightness of both images. A detailed description of this technique can be found in [10].

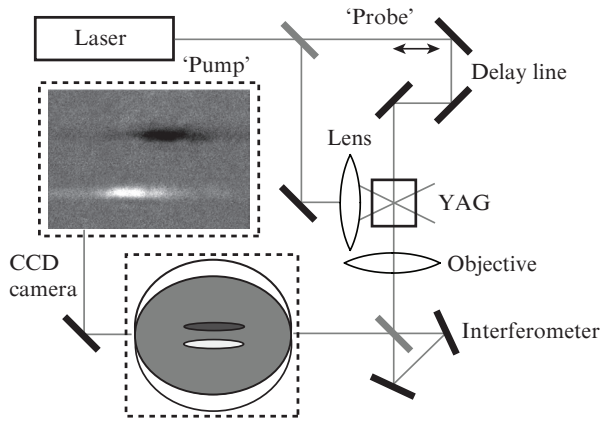

Figure 1. Irradiation scheme in femtosecond interferometry. The inset shows a typical interference pattern observed on CCD camera display.

3. Simulation

Experimental data were compared with the results of numerical simulation. The transmission of a laser pulse through a medium and excitation of the electron subsystem of YAG crystal was described by the system of equations

$$\frac{\partial E}{\partial z} = \frac{\mathrm{i}}{2k_0}\left(\frac{1}{r}\frac{\partial}{\partial r} + \frac{\partial^2}{\partial r^2}\right)E - \frac{\mathrm{i}k''}{2}\frac{\partial^2 E}{\partial t'^2} + \frac{\mathrm{i}k_0 n_2}{n_0}|E|^2 E - \frac{1}{2}\beta^{(5)}|E|^8 E + \frac{\mathrm{i}k_0}{n_0}n_\mathrm{t}\rho_\mathrm{t}E, \quad (1)$$

$$\frac{\partial \rho_\mathrm{t}}{\partial t'} = \frac{\beta^{(5)}}{5\hbar\omega_0}|E|^{10}. \quad (2)$$

Equation (1) is a wave equation for the complex electromagnetic field amplitude E in the slowly varying amplitude approximation (see, e.g., [11]). The first term on the right-hand side of Eqn (1) is the diffraction one. The second, third, and fourth terms correspond, respectively, to the group-velocity dispersion, nonlinear beam focusing due to the optical Kerr effect, and five-photon absorption. The fifth term describes the effect of radiation-induced short-lived bound states in YAG. As was shown in [10], bound states in YAG are generated directly during light absorption rather than through relaxation of free carriers (presumably, as well as in $CaWO_4$ crystals [12]). Equation (2) describes the generation of these states. Since their experimentally found lifetime turned out to be 150 ps [13], the relaxation was disregarded.

In Eqns (1) and (2), $t' \equiv t - n_0 z/c$; k_0 and ω_0 are the wave number and angular light frequency, respectively; $k'' = 98.5$ fs^2 cm^{-1} is the group-velocity dispersion [14]; $n_0 = 1.82$ is the linear refractive index of YAG; $n_2 = 6.5 \times 10^{-16}$ cm^2 W^{-1} is the nonlinear [15] refractive index of YAG; $\beta^{(5)} = 3.1 \times 10^{-51}$ cm^7 W^{-4} is the five-photon absorption coefficient [16]; ρ_t is the density of bound states; and $n_\mathrm{t}\rho_\mathrm{t}$ is the contribution of bound states to the refractive index. The parameter n_t was varied in the calculations. The calculation results presented below were obtained with $n_\mathrm{t} = 1.5 \times 10^{-24}$ cm^3. Note that a variation in n_t in the vicinity of this value or below it did not lead to any significant change in the results of solving system (1), (2).

The initial laser pulse had a Gaussian spatial and temporal shape with a width $\tau_\mathrm{FWHM} = 140$ fs; it was focused by a lens with a numerical aperture NA = 0.1 at a depth of 300 μm from the sample surface.

4. Reproduction of femtosecond interferometry data

To compare the results of numerical calculations with experimental data, we simulated the transmission of a probe pulse through the laser-irradiated region at different delay times t_d. To this end, the distribution of induced refractive index in YAG, $\Delta n(r,z,t) = n_2|E(r,z,t)|^2 + n_\mathrm{t}\rho_\mathrm{t}(r,z,t)$, with a transition to the laboratory time, was calculated. Then the phase delay

$$\Delta\varphi(x,z,t) = \frac{2\pi}{\lambda}\int_{-\infty}^{\infty}\Delta n\left(\sqrt{x^2+y^2}, z, t + \frac{n_0 y}{c}\right)\mathrm{d}y \quad (3)$$

was determined for a thin time layer of a probe pulse propagating along the Y axis, and a time convolution was performed:

$$B(x,z,t_\mathrm{d}) = I_0^\mathrm{p}\int_{-\infty}^{\infty}\sin[\Delta\varphi(x,z,t)]\exp\left[-\frac{(t+t_\mathrm{d})^2}{\tau^2}\right]\mathrm{d}t. \quad (4)$$

The thus obtained datasets $B(x,z)$ are interference photographs (reproduced in the calculations) corresponding to those experimentally obtained using the schematic presented in Fig. 1. Note that these photographs are idealised, because the calculations were performed disregarding the diffraction from thin objects, absorption, and imperfection of the optical system.

5. Results and discussion

The interference photographs recorded with different probe beam delays are shown in Fig. 2a. The pump pulse energy was 0.52 μJ. The bright regions correspond to positive phase shifts of the probe beam, i.e., positive values of induced refractive index. The bright wide 'cloud' moving from right to left is due to the optical Kerr effect; it is a pump pulse image. The narrow band at the centre of photographs corresponds to the region containing light-induced bound states. Note that intense femtosecond irradiation of YAG crystal does not lead to the occurrence of regions with a reduced refractive index, which occur in most solids as a result of free-carrier generation (see, for example, [17]).

The numerically calculated interference photographs are shown in Fig. 2b. The calculated and experimental images obtained with time delays of 0 and 350 fs are in good agreement. It can be seen that the pulse narrows and becomes more intense when approaching the focal region. Note that the pump pulse power at an energy of 0.52 μJ exceeds the critical power for self-focusing by a factor of almost 4; therefore, the beam focusing is significantly nonlinear in this case because of the optical Kerr effect.

When the pulse reaches the focal region (delay of 520 fs), diffraction bands can be observed in the experimental images. This diffraction is due to the presence of bound electronic states in the irradiated region. According to the calculations, the perturbed-region diameter is ~500 nm. The strong diffraction does not make it possible to compare quantitatively the experimental and theoretical data for the focal region; however, they are qualitatively consistent.

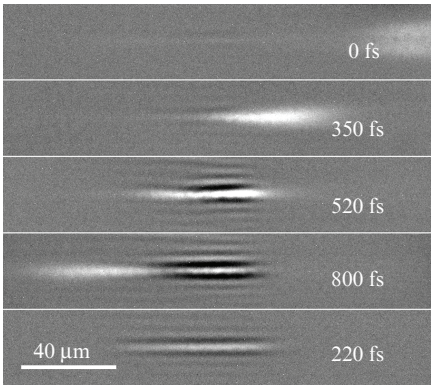

a

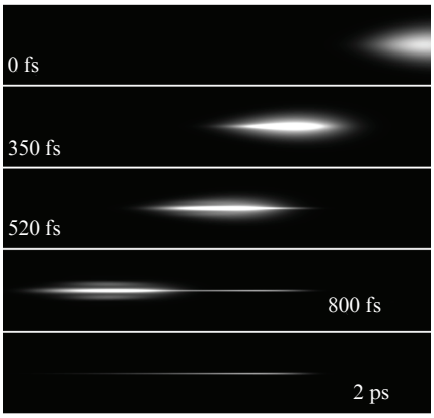

b

Figure 2. Interference photographs for a 0.52 μJ femtosecond laser pulse propagating (from right to left) in a YAG crystal: (a) experiment and (b) simulation.

When the pulse leaves the focal region (delay of 800 fs), the good correspondence between the calculated and experimental results is recovered. However, according to the simulation results, a secondary maximum (indistinguishable in the experiment) arises in the beam at this instant. Apparently, the reason is that the fine details of the observed pattern are obscured because of the insufficiently high spatial resolution of the optical system.

Thus, the low resolution of the optical system is a critical problem. To perform a quantitative comparison of the theoretical and experimental results, one must calculate more accurately the interference photographs, taking into account both the probe beam diffraction from subwavelength objects and the aberration of the optical system. Nevertheless, the above-reported data indicate that Eqns (1) and (2), which take into consideration the formation of short-lived bound states directly via five-photon absorption, describe correctly the light-induced processes occurring in the YAG crystal.

The calculations made it possible to trace, in particular, the change in the intensity and shape of the pump pulse during its passage through the focal region. Note that at powers above critical a typical regime of pulse propagation in the medium is filamentation [11], which is mainly due to the balance between the self-focusing of the beam and its defocusing by the free-carrier plasma. In the case of YAG crystal, the absence of defocusing led to a peculiar propagation regime, differing from the classical filamentation.

The spatial distribution of light intensity at the instants indicated in Fig. 2 is shown in Fig. 3. It can be clearly seen that the pulse shape changed significantly during motion through the focal region. The critical factor in this process was the five-photon absorption, which limited the intensity to a value not larger than 3.5×10^{13} W cm^{-2}. As a result of the interaction between the self-focusing and absorption processes, the propagating pulse narrowed in the radial direction and was essentially elongated both in the axial direction and in time. For example, at a time delay of 350 fs, the radius (at the 1/e level) and width (at half maximum) were, respectively, 1 μm and 100 fs. At a delay of 800 fs, the radius decreased to 0.8 μm, while the width increased to 200 fs. The beam propagated in this regime until its power decreased below the critical level, after which the beam became divergent due to diffraction.

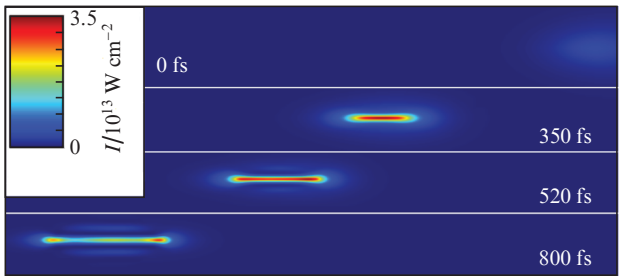

Figure 3. Change in the intensity of a 0.52 μJ pulse during its propagation through the focal region in the YAG bulk.

As was said above, a key condition for establishing and maintaining the aforementioned beam propagation regime is to limit the beam intensity via multiphoton absorption under strong self-focusing conditions. The characteristic self-focusing length is $L_{sf} = 1/(n_2 k_0 I)$ (see [11]), where I is the intensity on the beam axis. The characteristic length of K-photon absorption is $L_{mpa} = 1/(2\beta^{(K)} I^{K-1})$. It is reasonable to suggest that the rise in intensity under focusing conditions is suppressed when the values L_{sf} and L_{mpa} become close. Neglecting diffraction and other effects, one can propose the following formula to estimate (for $K \geqslant 3$) the intensity at which a balance between the absorption and self-focusing processes occurs:

$$I_{lim} = a^{(K)}[n_2 k_0/(2\beta^{(K)})]^Z. \quad (5)$$

Here, $Z = 1/(K-2)$; $a^{(K)}$ is a dimensionless factor on the order of unity.

To analyse the applicability of formula (5), we calculated the dependence of the saturation intensity I_{lim} on the five-photon absorption coefficient (Fig. 4). To this end, we used Eqn (1) disregarding the terms describing the group-velocity dispersion and refraction due to the occurrence of bound states. The $\beta^{(5)}$ value was varied from 3.1×10^{-52} to 3.1×10^{-50} cm^7 W^{-4}. The approximation of the dependence $I_{lim}(\beta^{(5)})$ by formula (5) at $Z = 1/3$ is shown by a dotted line; in this case, $a^{(5)} = 1.48$. The approximation with $Z = 1/3.5$ (the solid line) turned out to be much more exact. The observed discrepancy is related to the diffraction [disregarded when deriving estimation formula (5)].

Thus, a method for computer calculation of femtosecond interferometry photographs was proposed for correct comparison of experimental data and results of numerical simula-

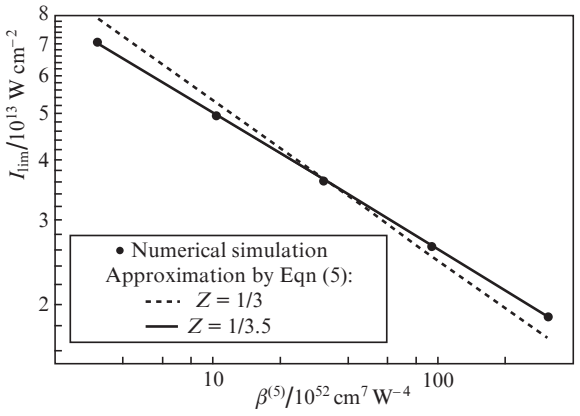

Figure 4. Calculated dependence of the saturation intensity on the five-photon absorption coefficient for a 0.52 μJ pulse.

tion of the interaction of femtosecond pulse with a medium. This approach showed good correspondence between the theory and experiment for yttrium aluminium garnet. A key problem remains to be the imperfection of interference photographs, which is primarily related to the probe beam diffraction. A numerical experiment demonstrated a regime of laser pulse propagation through a YAG crystal, in which the presence of Kerr self-focusing and absence of plasma defocusing led to strong beam narrowing and pulse elongation.

Acknowledgements. This work was supported by the Ministry of Education of the Russian Federation (Project No. 3.2608.2017/PCh).

References

1. Davis K.M., Miura K., Sugimoto N., Hirao K. *Opt. Lett*., **21**, 1729 (1996).
2. Griscom D.L., Gingerich M.E., Friebele E.J. *Phys. Rev. Lett*., **71**, 1019 (1993).
3. Rothschild M., Arnone C., Ehrlich D.J. *J. Vac. Sci. Technol*. **4**, 310 (1986).
4. Kononenko T.V., Zavedeev E.V. *Quantum Electron*., **46**, 229 (2016) [*Kvantovaya Elektron*., **46**, 229 (2016)].
5. Pavlov I., Tokel O., Pavlova S., Kadan V., Makey G., Turnali A., Yavuz Ö., Ilday F.Ö. *Opt. Lett*., **42**, 3028 (2017).
6. Shimotsuma Y., Kazansky P.G., Qiu J., Hirao K. *Phys. Rev. Lett*., **91**, 247405 (2003).
7. Juodkazis S., Misawa H., Hashimoto T., Gamaly E.G., Luther-Davies B. *Appl. Phys. Lett*., **88**, 201909 (2006).
8. Garnov S.V., Konov V.I., Malyutin A.A., Tsarkova O.G., Yatskovsky I.S., Dausinger F. *Laser Phys*., **13**, 386 (2003).
9. Azechi H., Oda S., Tanaka K., Norimatsu T., Sasaki T., Yamanaka T., Yamanaka C. *Phys. Rev. Lett*., **39**, 1144 (1977).
10. Zavedeev E.V., Kononenko V.V., Konov V.I. *Appl. Phys. A*, **123**, 499 (2017).
11. Couairon A., Mysyrowicz A. *Phys. Rep*., **441** (2–4), 47 (2007).
12. Nagirnyi V., Geoffroy G., Grigonis R., Guizard S., Kirm M., Kotlov A., Nagornaya L.L., Nikl M., Sirutkaitis V., Vielhauer S. *Radiat. Meas*., **45** (3–6), 262 (2010).
13. Kononenko V.V., Zavedeev E.V., Okhrimchuk A.G., Konov V.I. *Laser Phys. Lett*., **14**, 066002 (2017).
14. Zelmon D.E., Small D.L., Page R. *Appl. Opt*., **37**, 4933 (1998).
15. Takeuchi Y., Kawanaka J., Fujita M. *CLEO/Europe-EQEC 2009 Conf. Dig.* (Munich, 2009) CA_P24.
16. Okhrimchuk A.G., Mezentsev V.K., Schmitz H., Dubov M., Bennion I. *Laser Phys*., **19**, 1415 (2009).
17. Kononenko V.V., Zavedeev E.V., Latushko M.I., Pashinin V.P., Konov V.I., Dianov E.M. *Quantum Electron*., **42**, 925 (2012) [*Kvantovaya Elektron*., **42**, 925 (2012)].